analytical chemistry

pubs.acs.org/ac Article

MXene Titanium Carbide-based Biosensor: Strong Dependence of Exfoliation Method on Performance

Hui Ling Chia, Carmen C. Mayorga-Martinez, Nikolas Antonatos, Zdeněk Sofer, Jesus J. Gonzalez-Julian, Richard D. Webster, and Martin Pumera*

Cite This: https://dx.doi.org/10.1021/acs.analchem.9b03634 Read Online

ACCESS | Metrics & More | Article Recommendations | Supporting Information

ABSTRACT: Transition metal carbides, known as MXenes, are generated via the selective etching of "A" layers from their layered, ternary parent compounds, MAX phases, where M corresponds to early *d*-transition metal, A being a main group *sp*-element from either Group 13 or 14 and carbon or nitrogen being denoted by X. MXenes are being recognized as a new and uprising class of 2D materials with extraordinary physical and electrochemical properties. The huge specific surface area and outstanding electrical conductivity of MXenes, make them ideal candidates for sensing and energy applications. Herein, we demonstrated the successful incorporation of pristine MXene, Ti_3C_2 produced via HF etching and subsequent delamination with TBAOH, as a transducer platform toward the development of a second generation electrochemical glucose biosensor. Chronoamperometric studies demonstrate that the proposed biosensing system exhibits high selectivity and excellent electrocatalytic activity toward the detection of glucose, spanning over wide linear ranges of 50−27 750 μM and possess a low limit of detection of 23.0 μM. The findings reported in this study conceptually proves the probable applications of pristine MXenes toward the field of biosensors and pave ways for the future developments of highly selective and sensitive electrochemical biosensors for biomedical and food sampling applications.

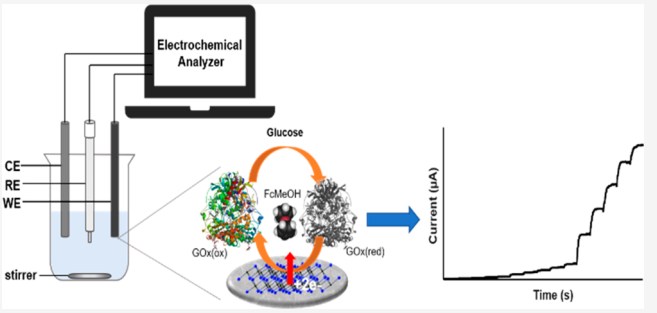

In recent years, the family of 2D materials has been extended by a novel and rapidly growing collection of early transition metal carbides known as MXenes.[1,2] MXenes are generated via the selective etching of "A" layers from their layered, ternary parent compounds, MAX phases. MAX phases possess a generic chemical formula of $M_{n+1}AX_n$, whereby M corresponds to early d-transition metal, A being a main group sp-element from either Group 13 or 14, and X corresponds to carbon or nitrogen.[3−7] M layers are closely arranged with X atoms lining amidst the octahedral sites and the $M_{n+1}X_n$ layers are sandwiched between layers of A atoms. The M−X bonds are found to be remarkably strong and possess a mixture of covalent, and ionic characteristics while M−A bonds are of a weaker nature and possess metallic characteristics.[1,8] As a consequence of weaker M−A bonds, it is possible to selectively remove the "A" layer from MAX phases via heat treatment under vacuum conditions or in molten salts or via chemical etching with hydrofluoric acid treatment. The selective etching of "A" layers yields $M_{n+1}X_nT_x$ layers (MXenes), whereby T_x are surface terminating moieties such as oxygen, hydroxyl or fluorine groups.[9−13] To date, more than 60 distinct types of pure MAX phases and 20 types of MXenes have been discovered. MXenes uniquely integrate the metallic-like conductivity inherited from their parent MAX phases and the hydrophilic nature of their surface terminating moieties. As a result of the unique mechanical, chemical, physical, and electrical properties presented by MXenes, vast amount of research has been conducted on MXenes to explore their utilities. MXenes show promising applications in numerous fields, such as transparent conductive films, supercapacitors, catalysts, electromagnetic interface shield, Li ion batteries, and sensors.[1,10,14−21]

Diabetes mellitus (DM) is listed among one of the most critical health challenges faced globally and is deemed as one of the foremost reasons causing mortality and disability throughout the globe.[22−24] The prevalence of DM is rapidly on the rise, whereby the number of people with DM was projected to rise from approximately 347 million people in 2013 to 552 million by 2030.[25] DM is a metabolic disorder that arises as a result of insulin deficiency and hyperglycemia, and is indicated by blood glucose concentrations larger than the conventional range of approximately 3.9−6.2 mM on an empty stomach or 3.9−7.8 mM 2 h after food consump-

Received: August 9, 2019
Accepted: January 14, 2020

tion.[23,26] The quantitative monitoring of glucose concentration in blood is cardinal for the diagnosis and management of DM, which can significantly reduce micro and macrovascular complications such as nephropathy, cardiovascular diseases, and retinopathy.[24,27,28] As a consequence, enormous effort has been devoted to develop glucose-measuring devices. Over the past decades, biosensor technology has seen numerous breakthroughs and plays a crucial role as a powerful analytical tool in the medical field. Glucose biosensors have been dominating the biosensor market and account for approximately 85% of the market share. Today, a vast majority of the commercially available glucose biosensors belong to the electrochemical class, because of their numerous advantages such as high sensitivity, ability to give a fast response, low cost of operation, and easy maintenance.[22,24,26,29,30]

Direct electron transfer (DET) between enzymes and electrodes is cardinal for the construction of electrochemical biosensors. However, electroactive centers are often deeply embedded within the protein core of enzymes, making it challenging for proteins to accomplish DET processes on the bare electrodes. To better facilitate the electrical contact amidst redox centers of glucose oxidase (GOx) and electrode surfaces and accelerate the transfer of electrons, various novel nanomaterials have been utilized for GOx immobilization.[26,31−34] MXenes possess numerous distinct properties, for instance large specific surface area and outstanding electrical conductivity, therefore MXenes could possibly be introduced as an efficient pathway to facilitate DET. Herein, we aspire to investigate the potential of incorporating MXenes toward the development of second generation electrochemical glucose biosensors. The heterogeneous electron transfer (HET) capabilities of bulk Ti_3AlC_2 and Ti_3C_2 synthesized via HF etching (Ti_3C_2−HF) and subsequent delamination by tetrabutylammonium hydroxide, TBAOH (Ti_3C_2−HF/TBA) were investigated and the superior material was then utilized to develop a glucose biosensor. Fabrication of the glucose biosensor was accomplished by pipetting MXene materials onto the surface of glassy carbon (GC) electrode, then glucose oxidase (GOx), and last cross-linking with glutaraldehyde (GTA) to yield the biosensor. The as-synthesized MXene-based biosensor allows selective, sensitive, and fast amperometric detection of glucose, as depicted in Scheme 1.

EXPERIMENTAL SECTION

Synthesis of Ti_3AlC_2. The MAX phase, Ti_3AlC_2, was synthesized by mixing Ti, Al, and graphite powders (Alfa Aesar) in stoichiometric molar ratio of 3:1:2 with KBr in a weight ratio of 1:1. The 24 h mixing process was carried out in a multidirectional mixer (Turbula, WAB, Switzerland), using ethanol as liquid media and 5 mm diameter zirconia milling balls. A steel die was then used to uniaxially pressed the dried powder mixture at a pressure of 200 MPa. The pressed powder was then subjected to further encapsulation with KBr and placed in an alumina crucible lined with KBr salt bed. The resulting mixture was heated at 1300 °C for an hour with a heating rate of 5 °C/min. Upon cooling, Ti_3AlC_2 was obtained by dissolving the reaction mixture in water and subsequent washing with hot water to eliminate the residual KBr salt content. Lastly to prevent agglomeration, the Ti_3AlC_2 powder was rinsed in ethanol, dried overnight at 70 °C in an oven and sieved through 63 μm sieve.

Synthesis of MXenes (Ti_3C_2−HF and Ti_3C_2−HF/TBA). Ti_3C_2−HF: 2g of Ti_3AlC_2 was immersed in 100 mL 40% HF solution (Sigma-Aldrich) and stirred continuously under ambient conditions for 7 days. After which, the samples were separated via repeated rounds of centrifugation and redispersion in water and subsequently via suction filtration. Thereafter, the etched sample was dried for 24 h in a vacuum oven set at 50 °C.

Ti_3C_2−HF/TBA: 1 g of Ti_3C_2−HF was stirred continually with 50 mL of 40% TBAOH (Sigma-Aldrich) under ambient conditions for an hour. The sample was then ultrasonicated for 0.5 h (12 L bath, 20 °C, 400 W), separated via suction filtration, followed by washing with deionized water. After which, the delaminated material was dried for 24 h in a vacuum oven set at 50 °C.

Scheme 1. Schematic Illustration Depicting the (a) Exfoliation of Ti_3AlC_2 to Generate Ti_3C_2−HF via Etching with HF (b) Delamination of Ti_3C_2−HF with TBAOH to yield Ti_3C_2−HF/TBA; Construction of the Proposed Glucose Biosensing System by (c) Modifying the Glassy Carbon Electrode with Ti_3C_2−HF/TBA, (d) Followed by Loading of Glucose Oxidase (GOx), and (e) Subsequently Cross-Linking Glutaraldehyde (GTA) with GOx; (f) Glucose Detection Mechanism of the Proposed Biosensing System

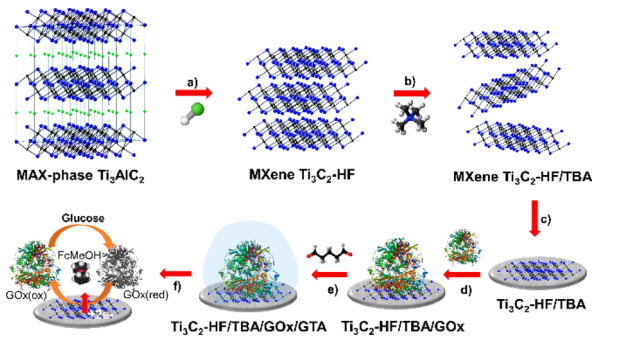

Biosensor Preparation. Prior to use, the surface of GC electrodes was renewed via polishing using a series of alumina particle slurry (9 μm, 5 μm, 1 μm, 0.3 μm sequentially) on a polishing pad. After which, the electrodes were rinsed with ultrapure water then dried via dry polishing on a polishing pad.

Ti_3AlC_2 or MXenes were added to dimethylformamide to yield separate 5 mg mL^{-1} suspensions and preceding each electrochemical measurement the suspension was ultrasonicated for 1 min to make certain that the material of interest is homogeneous. 0.75 μL of material suspension was then pipetted on the electrode surface and dried under ambient conditions. Subsequently, 0.1 mg of glucose oxidase (GOx) in ultrapure water (20 mg mL^{-1}) was pipetted onto the material modified electrode and similarly left to dry under ambient conditions. Lastly, 5 μL of 1% v/v glutaraldehyde solution was pipetted onto the electrode surface to cross-link the GOx enzyme and dried for an hour in an oven set at 35 °C. The final modified electrode denoted as Ti_3AlC_2/GOx/GTA/GC, Ti_3C_2−HF/GOx/GTA/GC and Ti_3C_2−HF/TBA/GOx/GTA/GC was kept at 4 °C when not in use.

Electrochemical Measurements. Voltammetric and chronoamperometric measurements were conducted via an Eco Chemie μAutolab type III electrochemical analyzer linked to a laptop and the parameters were set up via the NOVA version 1.10 software. All measurements in the study were performed under ambient conditions via the use of a three-electrode configuration in a 10 mL electrochemical glass cell

https://dx.doi.org/10.1021/acs.analchem.9b03634
Anal. Chem. XXXX, XXX, XXX−XXX

comprising of a modified glassy carbon working electrode, platinum counter electrode, and Ag/AgCl reference electrode.

Heterogeneous electron-transfer (HET) measurements were performed using cyclic voltammetry (CV) with potentials ranging from −0.2 to 0.5 V, a scan rate of 50 mV s^{-1} and 0.1 M KCl as supporting electrolyte for ferri/ferrocyanide redox probe (5 mM). Chronoamperometry measurements (Δt > 1 ms) were carried out at a constant potential of 0.15 V, whereby distinct glucose concentrations were added into the ferrocenemethanol solution (FcMeOH, 2 mM) at every 200 s intervals and the solution was continually stirred across the measurements. The data attained were smoothed and subsequently administered with baseline correction for further analysis.

RESULTS AND DISCUSSION

In order to synthesize the desired Ti_3C_2, Ti_3AlC_2 MAX phase was first synthesized by a molten salt process with Ti, Al, and graphite in stoichiometric molar ratio of 3:1:2 in KBr melt. The as-prepared Ti_3AlC_2 was then utilized to prepare MXenes via two routes; (1) etching with 40% hydrofluoric acid (HF) (2) etching with 40% HF followed by delamination with 40% TBAOH, termed Ti_3C_2−HF and Ti_3C_2−HF/TBA, respectively. The physical and chemical properties of the as-prepared MXene before etching, after etching, and after delamination were examined via transmission electron microscopy (TEM), energy X-ray dispersive spectroscopy (EDX), atomic force microscopy (AFM), X-ray diffraction spectroscopy (XRD), Raman, and X-ray photoelectron spectroscopy (XPS).

Transmission electron microscopy (TEM) was first utilized to investigate the morphological differences of Ti_3AlC_2 MAX phase, Ti_3C_2−HF, and Ti_3C_2−HF/TBA, induced by the exfoliation and delamination processes, and the data are illustrated as in Figure 1. Through the TEM images in Figure 1a, it is inferred that MAX phase displays structural features typical of bulk materials and manifest as micron sized flakes, while SAED and HRTEM studies reveal the hexagonal symmetry possessed by the material. TEM images of exfoliated Ti_3C_2−HF in Figure 1b show an expanded structure due to the etching of aluminum, whereas SAED and HRTEM show that the hexagonal symmetry of the material is still retained despite undergoing the etching process with hydrofluoric acid.

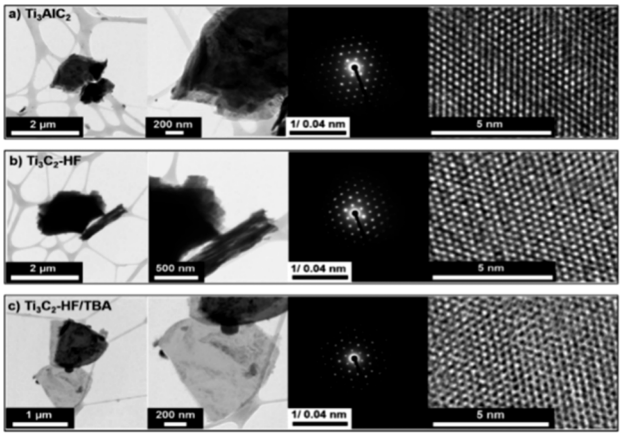

Figure 1. TEM images with corresponding SAED images and high resolution TEM images of (a) bulk Ti_3AlC_2, (b) exfoliated Ti_3C_2−HF, and (c) delaminated Ti_3C_2−HF/TBA.

Meanwhile, the delamination of Ti_3C_2−HF with TBAOH led to the formation of single and few-layer MXene (Ti_3C_2−HF/TBA) while retaining the hexagonal symmetry of the structure.

Next, we move on to ascertain the types of elements present in the materials and their distribution via the use of energy dispersive X-ray spectroscopy (EDX). Through the EDX elemental maps in Figure 2, it was observed that Ti, C, and Al corresponding to the composition of starting MAX phase are homogeneously distributed throughout the material. Subsequent exfoliation and delamination of the bulk MAX phase led to the removal of aluminum as depicted in Figure 2b and c and the introduction of surface terminating functional group containing oxygen and fluorine, which arises from the selective etching of reactive Al layers with hydrofluoric acid.

AFM measurements were performed to determine the thickness of Ti_3AlC_2 MAX phase, Ti_3C_2−HF and Ti_3C_2−HF/TBA. AFM data (see Supporting Information (SI) Figure S-1) suggest that the thickness of Ti_3AlC_2 ranges from 1 to 2 μm, confirming its bulk state. Meanwhile, Ti_3C_2−HF and Ti_3C_2−HF/TBA was measured to possess an average thickness range of ca. 5−6 nm and 1−3 nm, respectively, suggesting the successful etching and subsequent delamination of the Ti_3AlC_2 MAX phase.

In addition, XRD and Raman spectroscopy were also performed to determine the extent of exfoliation and are illustrated in SI Figures S-2 and S-3, respectively. As depicted in SI Figure S-2a, the XRD pattern obtained for bulk Ti_3AlC_2 is in good agreement with the data recorded in literature,[35] with peaks at 2θ values of 9.5°, 19.1°, 34°, 36.8°, 38.9°, 41.7°, 44.9°, 48.4°, 52.3°, 56.4°, and 60.1°, which have been assigned to the (002), (004), (101), (103), (104), (105), (106), (107), (108), and (110) planes, respectively. Upon treatment with 40% HF, there is a broadening of peaks and a decrease in peak intensities (see in SI Figures S-2b), which arises due to a decrease in the crystallinity and structural order of the material. Furthermore, the absence of nonbasal peaks especially (104) peak at 38.9°, indicates the successful etching of aluminum atoms from the bulk Ti_3AlC_2. In addition, a shift of the (002) and (004) peaks toward lower angles was also observed. The phenomenon arises due to an increase in d-spacing originating from the structural expansion during etching and removal of the Al atoms and substitution of Al atoms with functional groups containing oxygen or fluoride.[36]

The subsequent treatment of Ti_3C_2−HF with TBAOH led to delamination which resulted in a shift of the characteristic (002) peak from 9.2° to 6.2° 2θ and the peak at 27.6° to a higher 2θ angle of 30.7°, indicating the introduction of TBAOH atoms in the lattice of Ti_3C_2 and potential substitution of the functional groups mentioned above (Figure S-2c in SI). The significant shift of the (002) peak also indicates a much larger d-spacing.

The Raman spectra of Ti_3AlC_2 depicted in SI Figure S-3a, revealed its characteristic vibrational modes at 154, 262, 409, and 603 cm^{-1}, which coincides well with literature.[35] The exfoliation of the bulk Ti_3AlC_2 with HF results in a strong peak at 144 cm^{-1} along with three smaller peaks at 403, 513, and 628 cm^{-1}. These peaks are characteristic vibrational modes for anatase TiO_2 formed by MXene partial oxidation (Figure S-3b). The treatment with HF causes a substitution of Al atoms by OH- groups based on the following reactions:[35,37]

$$Ti_3AlC_2 + 3HF \rightarrow AlF_3 + \frac{3}{2}H_2 + Ti_3C_2$$

https://dx.doi.org/10.1021/acs.analchem.9b03634
Anal. Chem. XXXX, XXX, XXX−XXX

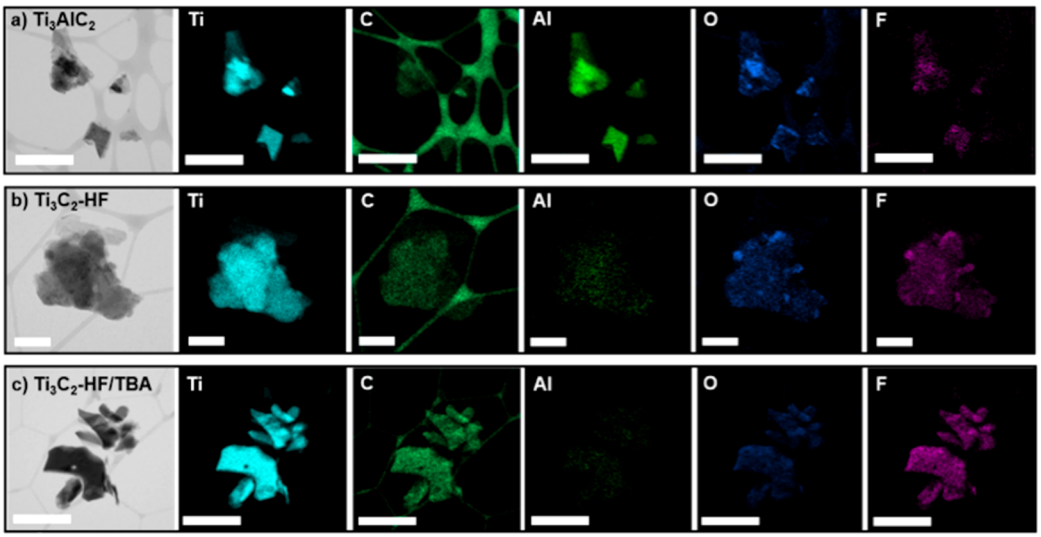

Figure 2. TEM images with corresponding EDX elemental distribution maps of (a) bulk Ti_3AlC_2, (b) exfoliated Ti_3C_2−HF, and (c) delaminated Ti_3C_2−HF/TBA. Scale bars correspond to 1 μm for Ti_3AlC_2 and Ti_3C_2−HF/TBA and 500 nm for Ti_3C_2−HF.

$$Ti_3C_2 + 2H_2O \rightarrow Ti_3C_2(OH)_2 + H_2$$

Meanwhile the treatment of Ti_3C_2−HF with TBAOH for an hour, causes the peak at 144 cm^{-1} to decrease drastically, and the three peaks between 400 and 700 cm^{-1} almost vanished (see Figure S-3c). These results suggest that the removal of anatase nanocrystals from exfoliated MXene surface was probably due to the delamination procedure.

In addition, XPS was conducted to study the surface composition of the bulk and exfoliated Ti_3AlC_2. Wide survey XPS spectra (see SI Figure S-4) confirmed the presence of the expected elements originating from the MAX compound (Ti, Al, C), while the presence of additional fluorine in Ti_3C_2−HF and Ti_3C_2−HF/TBA is a result of the exfoliation of the MAX phase with HF. Meanwhile, the atomic percentages of the elements present in the bulk Ti_3AlC_2, exfoliated and delaminated MXenes determined by XPS analysis are presented in SI Table S-1.

Analysis of the high-resolution XPS spectra (Figure 3) revealed the presence of a well-defined Ti 2p signal which is split into two binding energies of Ti $2p_{3/2}$ and Ti $2p_{1/2}$. Deconvolution of the Ti 2p peaks revealed that the dominant Ti peak for Ti_3AlC_2 etched with HF belongs to titanium oxide, whereas a significant decrease in percentage of titanium oxide and an increase in percentage of titanium carbide was observed for the delaminated product. (SI Table S-2) This is a further indication of the removal of anatase nanocrystals due to the delamination procedure. A comparison of Al 2s high-resolution XPS spectra is also presented (see SI Figure S-5) to demonstrate the successful removal of Al atoms via the exfoliation and subsequent delamination of the material.

Prior to the fabrication of the glucose biosensor, it is of utmost importance to assess the performances of Ti_3AlC_2 and MXenes (Ti_3C_2−HF and Ti_3C_2−HF/TBA) to evaluate any disparities in sensitivity and response to glucose based upon their distinct intrinsic properties. The HET rate is considered an important electrocatalytic parameter which determines the suitability of materials for sensing applications. HET rate is commonly associated with the peak-to-peak separation (ΔE_p), whereby small potential differences between the anodic and cathodic peaks generally equate to fast HET rates. Typically,

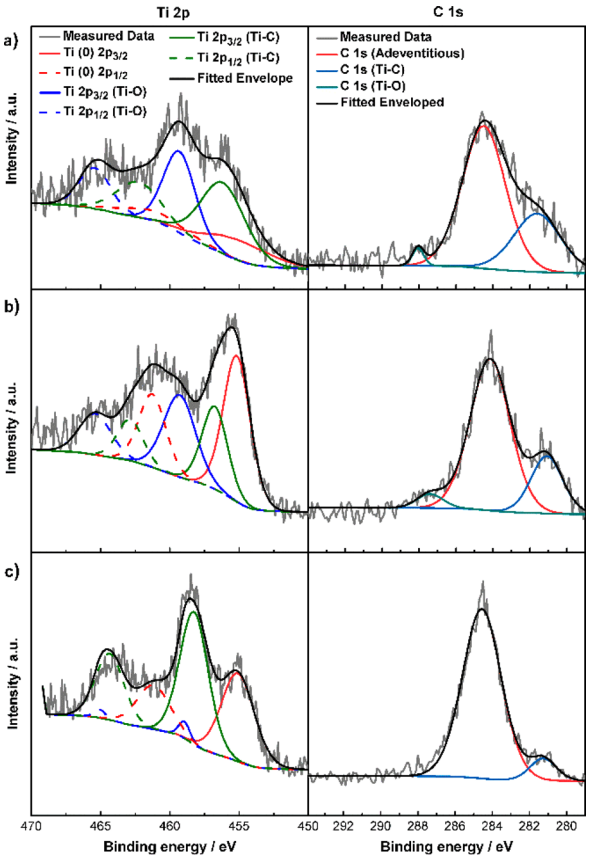

Figure 3. High resolution XPS spectra of (a) bulk Ti_3AlC_2, (b) exfoliated Ti_3C_2−HF, and (c) delaminated Ti_3C_2−HF/TBA.

materials with fast intrinsic HET rate are preferred to be used as electrode materials as they efficiently lessen the over-potentials needed for electrochemical reactions to occur.[38] As such, cyclic voltammetry was performed with a widely used ferro/ferricyanide redox probe to determine any differences in the heterogeneous electron-transfer (HET) capabilities of the materials. As depicted in Figure 4a, all materials have smaller ΔE_p as compared to GC, and the ΔE_p is ranked as follows:

https://dx.doi.org/10.1021/acs.analchem.9b03634
Anal. Chem. XXXX, XXX, XXX−XXX

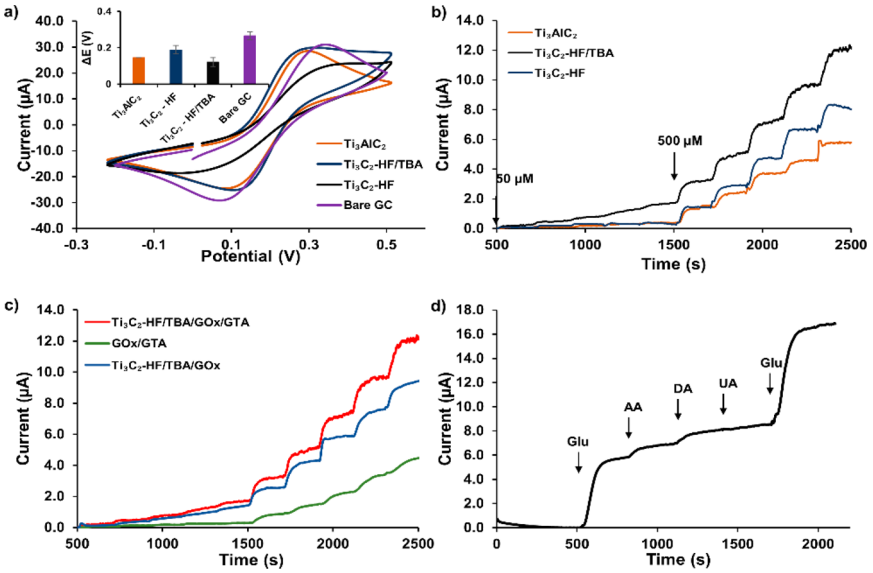

Figure 4. (a) Cyclic voltammograms of Ti_3AlC_2, Ti_3C_2−HF and Ti_3C_2−HF/TBA versus bare GC electrode, performed in 0.1 M KCl supporting electrolyte supplemented with 5 mM $[Fe(CN)_6]^{4-/3-}$ at a scan rate of 50 mV s^{-1} and the peak separations for the probe (inset). (b) Chronoamperometry data of the second-generation electrochemical glucose biosensor predicated on Ti_3AlC_2, Ti_3C_2−HF and Ti_3C_2−HF/TBA where 50 μM of glucose was added every 200 s for 1000 s followed by 500 μM addition at 200 s intervals for another 1000 s. Chronoamperometry measurements were conducted at 0.15 V in PBS (pH 7.2) supplemented with 2 mM of FcMeOH. (c) Chronoamperometry data of the different electrode configurations of the propose second-generation electrochemical glucose biosensor, where 50 μM of glucose was added every 200 s for 1000 s followed by 500 μM addition at 200 s intervals for another 1000 s. Chronoamperometry measurements were conducted at 0.15 V in PBS (pH 7.2) supplemented with 2 mM of FcMeOH. (d) Chronoamperometry data obtained from the interference studies of Ti_3C2-HF/TBA biosensors, whereby successive addition of 5 mM glucose, 0.2 mM L-ascorbic acid, 0.2 mM dopamine hydrochloride, 0.2 mM uric acid, and 5 mM glucose occurs at every 300 s. The measurement was carried out in pH 7.2 PBS supplemented with 2 mM FcMeOH at 0.15 V potential.

Ti_3C_2−HF/TBA < Ti_3AlC_2 < Ti_3C_2−HF. The data suggest that all three materials have HET rates that are faster than GC and with the smallest ΔE_p, Ti_3C_2−HF/TBA, would have the fastest HET rate and would thus present superior electrocatalytic performance for sensing devices.

Upon determining the HET capabilities, second-generation titanium carbide-based glucose biosensors are fabricated, and their response behavior toward glucose detection are assessed. In second generation glucose biosensors, oxygen is replaced with nonphysiological mediators, which allows an enhancement in the transferring of electron to the electrode surface as FcMeOH is minute enough to access the thoroughly embedded flavin adenine dinucleotide (FAD) redox center. The glucose detection mechanism of a typical second-generation biosensor is initiated via an electron transfer from glucose to the catalytic FAD core of GOx (eq 1). Subsequently, FAD-GOx is regenerated via the intervention of FcMeOH as the mediator (eq 2), to generate ferrocenium ion (Fc^+MeOH), and lastly an oxidation signal corresponding to the glucose concentration is generated when Fc^+MeOH oxidizes at the electrode to regenerate the mediator FcMeOH (eq 3).[24,26,39,40]

$$\text{glucose} + \text{FAD} - \text{GOx} + \frac{1}{2}O_2 \rightarrow \text{gluconic acid} + \text{FADH}_2 - \text{GOx} + H_2O_2 \quad (1)$$

$$\text{FADH}_2 - \text{GOx} + 2\text{Fc}^+\text{MeOH} \rightarrow \text{FAD} - \text{GOx} + 2\text{FcMeOH} + 2\text{H}^+ \quad (2)$$

$$2\text{FcMeOH} \rightarrow 2\text{Fc}^+\text{MeOH} + 2\text{e}^- \quad (3)$$

Upon determining the inherent HET capabilities of the materials, we then move on to explore the feasibility of the suggested biosensing system to detect glucose and examine the performances of Ti_3AlC_2 and MXenes (Ti_3C_2−HF and Ti_3C_2−HF/TBA) toward glucose detection. To evaluate the response and determine any differences in sensitivity of the glucose biosensing system fabricated using Ti_3AlC_2 and MXenes, chronoamperometric measurements were carried out with sequential addition of glucose. From Figure 4b, the glucose detection responses among the materials compared are ostensibly distinct, whereby Ti_3C_2−HF/TBA yielded the largest response, accompanied by Ti_3AlC_2 then Ti_3C_2−HF. The chronoamperometry data trend is in good agreement with the HET study whereby Ti_3C_2−HF/TBA indeed yields the finest electrocatalytic performance for glucose sensing among the three materials compared. One plausible reason that could account for the superior performance of Ti_3C_2−HF/TBA, could be ascribed to the thinness and huge surface area of the materials. Delamination of Ti_3C_2−HF with TBAOH led to the formation of single and few layers Ti_3C_2−HF/TBA, which decreases the distance between the enzyme and the electrode as compared to the bulk and exfoliated counterparts, allowing efficient electron transfer between the electrode and enzyme. Furthermore, the larger surface area to volume ratio provides more active surface area available for protein binding and entrapment of substrates, thus permitting the access of a large quantity and homogeneous distribution of enzymes to be immobilized on the nanosheet.[8] Additionally, MXenes inherit the metallic nature of their parent MAX phases which endows them with excellent conductivity. The delamination process causes the removal of surface terminating groups on the MXene which further enhances the electrical conductivity of the MXene material and thus better facilitating the electron transfer process between the electrode and the enzyme.[8,11,41] Motivated by the excellent electrochemical properties of the

https://dx.doi.org/10.1021/acs.analchem.9b03634
Anal. Chem. XXXX, XXX, XXX−XXX

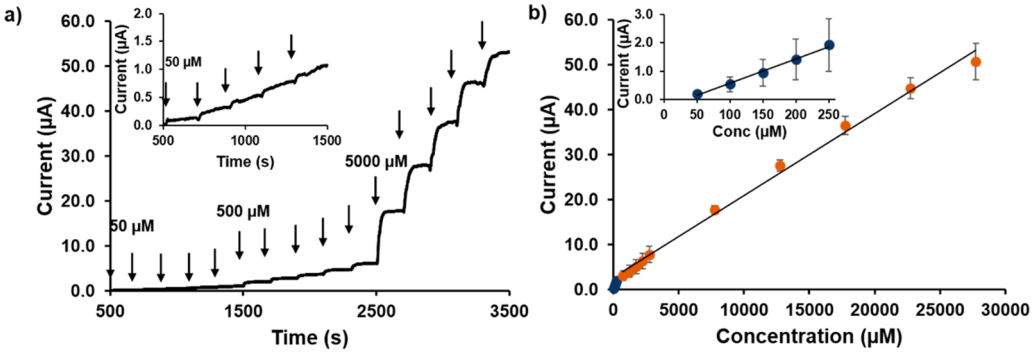

Figure 5. Chronoamperometry data (a) and calibration plot (b) for Ti_3C_2−HF/TBA-based electrochemical glucose biosensor conducted using FcMeOH (2 mM) in pH 7.2 PBS (electrolyte) and 0.15 V potential.

Ti_3C_2−HF/TBA, this material was selected to develop a second-generation glucose biosensor for subsequent studies.

In order to yield a comprehensive understanding and verify the roles of each respective component, individual biosensor component was examined via chronoamperometry measurements through sequential introduction of glucose to the different modified layers. Chronoamperometric responses were recorded and depicted in Figure 4c. The significance of enzyme GOx as the biorecognition element of glucose is evident, as it triggers the detection mechanism and generate distinct responses after injection of glucose (green curve) and along with Ti_3C_2−HF/TBA, GOx signal increases even more significantly (blue curve) when MXene was introduced. Very often, the sensing capability of amperometric glucose biosensors is limited by the electron transfer process amidst GOx active sites and the electrode surfaces. Due to the thick layer of protein enveloping the FAD redox center, an inherent barrier toward direct electron transfer is being introduced and hence GOx are unable to transfer electrons directly to traditional GC electrodes. As such, several innovative measures including the use of nanomaterials with extraordinary electrical property and large specific surface area have been looked into in order to construct and enhance the electrical contact amidst the FAD core of GOx and electrode surfaces.[23,37] MXenes have been reported to have excellent conductivity and its huge surface area significantly increases the active surface area for proteins to bind onto and substrate entrapment.[33] As such, the Ti_3C_2−HF/TBA could have possibly aid in ameliorating the sensitivity and response signal of the glucose sensing platform, hence enhancing the signal. The performance of the biosensor is further enhanced upon the addition of glutaraldehyde (red curve) as glutaraldehyde aids in the cross-linking of matrixes to help GOx maintain its structural rigidity, entraps and stabilizes the Ti_3C_2−HF/TBA and GOx layers on the GC electrode.

Having verified the feasibility of the enzymatic glucose biosensor platform, we moved on to examine if commonly found interferences would cause any probable signal induction on the proposed system to determine its selectivity. Chronoamperometric analysis was carried out with the following interferences; 0.2 mM of L-ascorbic, 0.2 mM of dopamine hydrochloride, and 0.2 mM of uric acid. These compounds were selected as they are commonly present in blood and are electrochemically active.[29,41−43] As depicted in Figure 4d, the addition of interfering compounds did not give rise to significant current changes, whereas a well-defined response is observed with additions of glucose, thus validating the use of a low working potential. This exemplary selectivity can be attributed to the fact that the biosensing system likely reacts preferentially with glucose rather than other compounds. Utilizing the information obtained, we next set forth to perform subsequent chronoamperometry measurements at 0.15 V.

Upon optimizing the parameters, the analytical response of the biosensing system was then evaluated via chronoamperometry, whereby distinct concentrations of glucose were sequentially introduced and continually stirred into PBS (pH 7.2) supplemented with 2 mM of FcMeOH. As depicted in Figure 5a, increasing the concentration of glucose causes an increase in oxidation current. Meanwhile, the linear plot for glucose concentrations between 50 and 27 750 μM is displayed in Figure 5b, whereby it shows that the Ti_3C_2−HF/TBA-based biosensing system detects glucose over two linear ranges, 50−250 μM (r = 0.997) and 750−27 750 μM (r = 0.997). Utilizing the approach define by IUPAC,[44−46] the limit of detection (LOD) was computed by multiplying the ratio between the standard deviation of the chronoamperometric signal obtained from the lowest concentration of glucose and the gradient attained from the calibration plot by a factor of 3, whereas limit of quantification (LOQ) is acquired by multiplication with a factor of 10. The biosensor was found to have a low LOD and LOQ of 23.0 and 76.8 μM, respectively, which demonstrates its high sensitivity for glucose detection.

Lastly, the proposed MXene-based glucose biosensor was tested with real samples to determine its feasibility for biomedical and food applications. Human serum containing 3.33−7.78 mM of glucose was acquired from Sigma-Aldrich,[47] introduced to the electrolyte solution, and the response generated was recorded. The glucose concentration of the serum was extrapolated from the calibration plot and calculated to be 1.83 ± 0.27 mM (n = 3). Recovery experiments were also performed to demonstrate the practicality of using the fabricated biosensors with real samples for food analysis. A recovery percentage of 95.2% was attained at glucose concentration of 500 μM in a sugar-free drink bought from a local grocer. These results attained imply that the fabricated glucose biosensing system could possibly be applied for real samples testing.

To yield a more comprehensive understanding of the proposed glucose biosensor performance, a comparison of analytical parameters with 2D materials-based biosensors presented in literature are summarized in Table 1. Gold nanoparticles have demonstrated unique abilities to provide enzymes with suitable microenvironments to retain their biological activity during immobilization processes and further

https://dx.doi.org/10.1021/acs.analchem.9b03634
Anal. Chem. XXXX, XXX, XXX−XXX

Table 1. Comparison of the Analytical Performances of the GC/Ti_3C_2−HF/TBA/GOx/GTA Glucose Biosensor with Other Electrochemical Glucose Biosensors Predicated on Layered Materials

electrode	linear range (μM)	LOD (μM)	ref
GC/Ti_3C_2−HF/TBA/GOx/GTA	50−250	23.0	this work
	750−27,750		
GC/MXene/Au/Nafion/GOx	100−18,000	5.9	48
GC/WS_2/GOx/GTA	180−770	82.6	29
	1300−7,600		
	7,600−22,300		
GC/WSe_2/GOx/GTA	77−274	52.0	
	770−22,300		
GC/Graphene/AuNPs/GOx	20−2,360	4.10	49
GC/MoS2/AuNPs/GOx	250−13,200	0.042	50

promote the transfer of electrons between the redox center of the immobilized biocatalyst and the electrode substrates.[51−53] As such pretreatment of layered materials with Au nanoparticles were commonly reported for 2D materials-based electrochemical glucose biosensors (Table 1), in the hope of improving the sensing performance of the biosensors, yielding lower detection limits. Though many of these biosensors yielded high sensitivity, some of their linear ranges fall out of the levels commonly reported in physiological fluids. In this work, we were able to present a second-generation glucose biosensor based simply upon pristine MXene (Ti_3C_2−HF/TBA), with performances being on par with or even better than several of the best published performances without having the need to pretreat MXene with Au nanoparticles. The delaminated MXene possess extraordinary electrochemical properties which greatly enhance the electron transfer process amidst the enzyme and the electrode, endowing the biosensor with excellent sensing performance and high sensitivity, outperforming biosensor based simply upon transition metal dichalcogenides.[29] Our proposed biosensing system offers linear ranges spanning over different magnitudes of glucose concentration and low LOD, proffering flexibility for the development of future electrochemical biosensors with high sensitivity for a wide variety of applications, ranging from biomedical to food analysis.

CONCLUSION

Inspired by the huge specific surface area and outstanding electrical properties of MXenes, we set forth to investigate the feasibility of incorporating MXene into a second-generation electrochemical glucose biosensor. In this work, we first investigated the inherent HET capabilities of the MAX and MXene materials and found that Ti_3C_2−HF/TBA (produced from etching of MAX phase with HF followed by subsequent delamination with TBAOH) gives rise to the smallest ΔE_p, has the fastest HET rate, and would present superior electrocatalytic performance for sensing devices. Motivated by the excellent electrochemical properties of Ti_3C_2−HF/TBA, this material was selected to develop a second-generation glucose biosensor. Chronoamperometric studies show that the proposed biosensing system exhibits high selectivity and outstanding electrocatalytic activity toward the detection of glucose, spanning over a wide linear range, and possessing a low limit of detection of 23.0 μM. The findings reported in this study conceptually proves the probable applications of pristine MXenes for future developments of highly selective and sensitive electrochemical biosensors for biomedical and food sampling applications.

ASSOCIATED CONTENT

Supporting Information

The Supporting Information is available free of charge at https://pubs.acs.org/doi/10.1021/acs.analchem.9b03634.

Description of characterization techniques performed. AFM images, XRD, Raman and wide survey XPS spectra of bulk Ti_3AlC_2, Ti_3C_2−HF, and Ti_3C_2−HF/TBA, comparison of high resolution Al 2p XPS spectra of Ti_3AlC_2 and Ti_3C_2−HF/TBA, tables displaying the atomic percentages of elements and atomic percentages of deconvoluted titanium peaks present in Ti_3AlC_2, Ti_3C_2−HF, and Ti_3C_2−HF/TBA obtained via XPS analysis (PDF)

AUTHOR INFORMATION

Corresponding Author

Martin Pumera − *Center for Advanced Functional Nanorobots, Department of Inorganic Chemistry, Faculty of Chemical Technology, University of Chemistry and Technology Prague, 166 28 Prague 6, Czech Republic; Department of Medical Research, China Medical University Hospital, China Medical University, Taichung, Taiwan; Future Energy and Innovation Laboratory, Central European Institute of Technology, Brno University of Technology, Brno CZ-616 00, Czech Republic; Department of Chemical and Biomolecular Engineering, Yonsei University, Seoul 03722, Korea;* orcid.org/0000-0001-5846-2951; Email: pumera.research@gmail.com

Authors

Hui Ling Chia − *NTU Institute for Health Technologies, Interdisciplinary Graduate School and Division of Chemistry and Biological Chemistry, School of Physical and Mathematical Sciences, Nanyang Technological University, 637553, Singapore*

Carmen C. Mayorga-Martinez − *Center for Advanced Functional Nanorobots, Department of Inorganic Chemistry, Faculty of Chemical Technology, University of Chemistry and Technology Prague, 166 28 Prague 6, Czech Republic;* orcid.org/0000-0003-3687-0035

Nikolas Antonatos − *Department of Inorganic Chemistry, University of Chemistry and Technology Prague, 166 28 Prague 6, Czech Republic;* orcid.org/0000-0003-2563-9970

Zdeněk Sofer − *Department of Inorganic Chemistry, University of Chemistry and Technology Prague, 166 28 Prague 6, Czech Republic;* orcid.org/0000-0002-1391-4448

Jesus J. Gonzalez-Julian − *Institute of Energy and Climate Research (IEK-1), Forschungszentrum Jülich, 52425 Jülich, Germany*

Richard D. Webster − *Division of Chemistry and Biological Chemistry, School of Physical and Mathematical Sciences, Nanyang Technological University, Singapore 637371;* orcid.org/0000-0002-0896-1960

Complete contact information is available at: https://pubs.acs.org/10.1021/acs.analchem.9b03634

Notes

The authors declare no competing financial interest.

https://dx.doi.org/10.1021/acs.analchem.9b03634
Anal. Chem. XXXX, XXX, XXX−XXX

■ ACKNOWLEDGMENTS

M.P. acknowledges the financial support of Grant Agency of the Czech Republic (EXPRO: 19-26896X). Z.S. was supported by the Neuron Foundation for scientific support.

■ REFERENCES

(1) Naguib, M.; Mochalin, V. N.; Barsoum, M. W.; Gogotsi, Y. *Adv. Mater.* **2014**, *26*, 992−1005.
(2) Zhu, J.; Ha, E.; Zhao, G.; Zhou, Y.; Huang, D.; Yue, G.; Hu, L.; Sun, N.; Wang, Y.; Lee, L. Y. S.; et al. *Coord. Chem. Rev.* **2017**, *352*, 306−327.
(3) Barsoum, M. W.; Radovic, M. *Annu. Rev. Mater. Res.* **2011**, *41*, 195−227.
(4) Anasori, B.; Xie, Y.; Beidaghi, M.; Lu, J.; Hosler, B. C.; Hultman, L.; Kent, P. R. C.; Gogotsi, Y.; Barsoum, M. W. *ACS Nano* **2015**, *9*, 9507−9516.
(5) Hu, C.; Zhang, H.; Li, F.; Huang, Q.; Bao, Y. *Int. J. Refract. Hard Met.* **2013**, *36*, 300−312.
(6) Xiao, B.; Li, Y.-c.; Yu, X.-f.; Cheng, J.-b. *Sens. Actuators, B* **2016**, *235*, 103−109.
(7) Dash, A.; Vaßen, R.; Guillon, O.; Gonzalez-Julian, J. *Nat. Mater.* **2019**, *18*, 465−470.
(8) Sinha, A.; Dhanjai; Zhao, H.; Huang, Y.; Lu, X.; Chen, J.; Jain, R. *TrAC, Trends Anal. Chem.* **2018**, *105*, 424−435.
(9) Tang, H.; Hu, Q.; Zheng, M.; Chi, Y.; Qin, X.; Pang, H.; Xu, Q. *Prog. Nat. Sci.* **2018**, *28*, 133−147.
(10) Ma, Y.; Liu, N.; Li, L.; Hu, X.; Zou, Z.; Wang, J.; Luo, S.; Gao, Y. *Nat. Commun.* **2017**, *8*, 1207.
(11) Shahzad, F.; Alhabeb, M.; Hatter, C. B.; Anasori, B.; Man Hong, S.; Koo, C. M.; Gogotsi, Y. *Science* **2016**, *353*, 1137−1140.
(12) Shen, B. S.; Wang, H.; Wu, L. J.; Guo, R. S.; Huang, Q.; Yan, X. B. *Chin. Chem. Lett.* **2016**, *27*, 1586−1591.
(13) Sarycheva, A.; Polemi, A.; Liu, Y.; Dandekar, K.; Anasori, B.; Gogotsi, Y. *Sci. Adv.* **2018**, *4*, eaau0920.
(14) Khazaei, M.; Ranjbar, A.; Arai, M.; Sasaki, T.; Yunoki, S. *J. Mater. Chem. C* **2017**, *5*, 2488−2503.
(15) Bai, X.; Ling, C.; Shi, L.; Ouyang, Y.; Li, Q.; Wang, J. *Sci. Bull.* **2018**, *63*, 1397−1403.
(16) Berdiyorov, G. R. *EPL* **2015**, *111*, 67002.
(17) Huang, K.; Li, Z.; Lin, J.; Han, G.; Huang, P. *Chem. Soc. Rev.* **2018**, *47*, 5109−5124.
(18) Hantanasirisakul, K.; Zhao, M.-Q.; Urbankowski, P.; Halim, J.; Anasori, B.; Kota, S.; Ren, C. E.; Barsoum, M. W.; Gogotsi, Y. *Adv. Electron. Mater.* **2016**, *2*, 1600050.
(19) Eklund, P.; Rosen, J.; Persson, P. O. Å. *J. Phys. D: Appl. Phys.* **2017**, *50*, 113001.
(20) Li, Y.; Deng, X.; Tian, J.; Liang, Z.; Cui, H. *Appl. Mater. Today* **2018**, *13*, 217−227.
(21) Zhu, J.; Chroneos, A.; Eppinger, J.; Schwingenschlögl, U. *Appl. Mater. Today* **2016**, *5*, 19−24.
(22) Newman, J. D.; Turner, A. P. F. *Biosens. Bioelectron.* **2005**, *20*, 2435−2453.
(23) Chen, C.; Xie, Q.; Yang, D.; Xiao, H.; Fu, Y.; Tan, Y.; Yao, S. *RSC Adv.* **2013**, *3*, 4473−4491.
(24) Yoo, E.-H.; Lee, S.-Y. *Sensors* **2010**, *10*, 4558−4576.
(25) Misra, R. D. K. *Mater. Technol. (London, U. K.)* **2015**, *30*, B140−B149.
(26) Wang, J. *Chem. Rev.* **2008**, *108*, 814−825.
(27) The Emerging Risk Factors, C.. *Lancet* **2010**, *375*, 2215−2222.
(28) Witkowska Nery, E.; Kundys, M.; Jeleń, P. S.; Jönsson-Niedziółka, M. *Anal. Chem.* **2016**, *88*, 11271−11282.
(29) Rohaizad, N.; Mayorga-Martinez, C. C.; Sofer, Z.; Pumera, M. *ACS Appl. Mater. Interfaces* **2017**, *9*, 40697−40706.
(30) Ping, J.; Fan, Z.; Sindoro, M.; Ying, Y.; Zhang, H. *Adv. Funct. Mater.* **2017**, *27*, 1605817.
(31) Kang, X.; Wang, J.; Wu, H.; Aksay, I. A.; Liu, J.; Lin, Y. *Biosens. Bioelectron.* **2009**, *25*, 901−905.
(32) Unnikrishnan, B.; Palanisamy, S.; Chen, S.-M. *Biosens. Bioelectron.* **2013**, *39*, 70−75.
(33) Liu, H.; Duan, C.; Yang, C.; Shen, W.; Wang, F.; Zhu, Z. *Sens. Actuators, B* **2015**, *218*, 60−66.
(34) Deng, S.; Jian, G.; Lei, J.; Hu, Z.; Ju, H. *Biosens. Bioelectron.* **2009**, *25*, 373−377.
(35) Naguib, M.; Kurtoglu, M.; Presser, V.; Lu, J.; Niu, J.; Heon, M.; Hultman, L.; Gogotsi, Y.; Barsoum, M. W. *Adv. Mater.* **2011**, *23*, 4248−4253.
(36) Zhao, C.; Wang, Q.; Zhang, H.; Passerini, S.; Qian, X. *ACS Appl. Mater. Interfaces* **2016**, *8*, 15661−15667.
(37) Swamy, V.; Kuznetsov, A.; Dubrovinsky, L. S.; Caruso, R. A.; Shchukin, D. G.; Muddle, B. C. *Phys. Rev. B: Condens. Matter Mater. Phys.* **2005**, *71*, 184302.
(38) Eng, A. Y. S.; Ambrosi, A.; Sofer, Z.; Šimek, P.; Pumera, M. *ACS Nano* **2014**, *8*, 12185−12198.
(39) Wang, J. *Electroanalysis* **2001**, *13*, 983−988.
(40) Mayorga-Martinez, C. C.; Sofer, Z.; Pumera, M., Binary Phosphorene Redox Behavior in Oxidoreductase Enzymatic Systems. *ACS Nano* **2019**.1313217
(41) Lorencova, L.; Bertok, T.; Dosekova, E.; Holazova, A.; Paprckova, D.; Vikartovska, A.; Sasinkova, V.; Filip, J.; Kasak, P.; Jerigova, M.; et al. *Electrochim. Acta* **2017**, *235*, 471−479.
(42) Wang, J.; Liu, J.; Chen, L.; Lu, F. *Anal. Chem.* **1994**, *66*, 3600−3603.
(43) Jia, W.-Z.; Wang, K.; Xia, X.-H. *TrAC, Trends Anal. Chem.* **2010**, *29*, 306−318.
(44) Long, G. L.; Winefordner, J. D. *Anal. Chem.* **1983**, *55* (7), 712A−724A.
(45) Riley, C. M., Chapter 2 Statistical Parameters and Analytical Figures of Merit. In *Progress in Pharmaceutical and Biomedical Analysis*; Riley, C. M.; Rosanske, T. W., Eds.; Elsevier, 1996; Vol. *3*, pp 15−71.
(46) Swartz, M.; Krull, I. *Handbook of Analytical Validation* **2012**, 61−80.
(47) Human Serum H4522. http://www.sigmaaldrich.com/catalog/product/sigma/h4522?lang=en&ion=SG.
(48) Rakhi, R. B.; Nayak, P.; Xia, C.; Alshareef, H. N. *Sci. Rep.* **2016**, *6*, 36422.
(49) Cao, X.; Ye, Y.; Li, Y.; Xu, X.; Yu, J.; Liu, S. *J. Electroanal. Chem.* **2013**, *697*, 10−14.
(50) Parlak, O.; İncel, A.; Uzun, L.; Turner, A. P. F.; Tiwari, A. *Biosens. Bioelectron.* **2017**, *89*, 545−550.
(51) Shan, C.; Yang, H.; Han, D.; Zhang, Q.; Ivaska, A.; Niu, L. *Biosens. Bioelectron.* **2010**, *25*, 1070−1074.
(52) Chen, Y.; Li, Y.; Sun, D.; Tian, D.; Zhang, J.; Zhu, J.-J. *J. Mater. Chem.* **2011**, *21*, 7604−7611.
(53) Ju, H. *Appl. Mater. Today* **2018**, *10*, 51−71.

https://dx.doi.org/10.1021/acs.analchem.9b03634
Anal. Chem. XXXX, XXX, XXX−XXX